Graphical Abstract

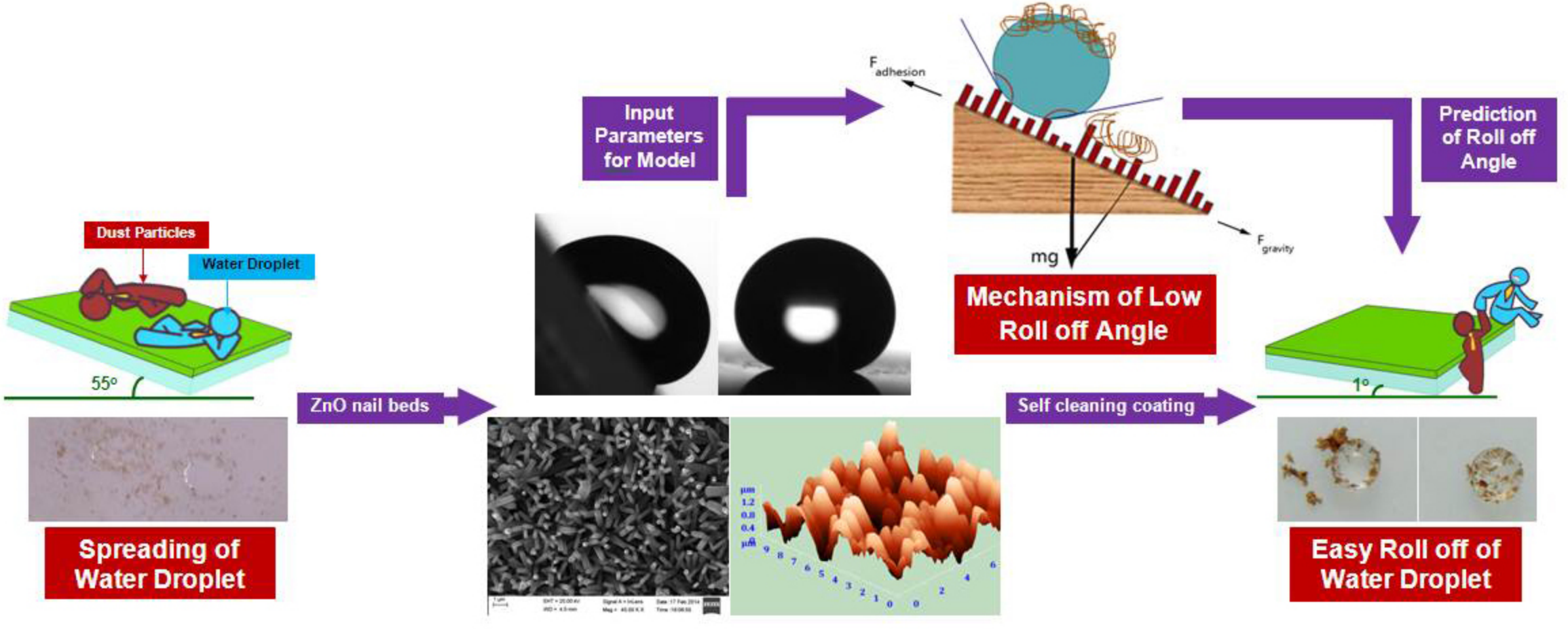

Studies on the influence of surface morphology of ZnO nail beds on easy roll off of water droplets

S. Sutha[1], S. C. Vanithakumari[2], R. P. George[2], U. Kamachi Mudali[2], Baldev Raj[3], K. R. Ravi[1*]

[1]PSG Institute of Advanced Studies, Coimbatore 641 004, Tamil Nadu, India.

[2]Corrosion Science and Technology Group, Indira Gandhi Centre for Atomic Research, Kalpakkam-603 102, Tamil Nadu, India.

[3]National Institute of Advanced Studies, Bangalore- 560 012, Karnataka, India.

*Corresponding Author: Tel: + 91 – 422 – 4344104, Fax: + 91 – 422 – 257 3833

Email: krravi.psgias@gmail.com

Abstract

A ZnO nanorods based superhydrophobic surface with extremely low roll-off values is fabricated using a two-step solution based approach- Successive Ionic Layer Adsorption and Reaction (SILAR) and Chemical Bath Deposition (CBD). The grown ZnO nanorods have average diameter of 285 nm with **a** predominant growth direction of [002]. The static contact angle of ZnO nanorods superhydrophobic surface is 155°**,** and the dynamic contact angles ~~such as~~ contact angle hysteresis and roll-off angle is 2° and 1° respectively. **Furthermore, to comprehend the mechanism governing the extremely low roll-off angle of ZnO nanorods based superhydrophobic surface,** ~~A~~an analytical model has been developed by incorporating the topographical (diameter, density of nanorods and solid area fraction) and droplet parameters (surface tension, mass and volume) ~~to understand the mechanism associated with the extremely low roll-off angle of ZnO nanorods based superhydrophobic surface~~. The theoretically calculated roll-off angle closely matches **with** the experimental results and ~~other~~ **reported** results ~~reported in the literature~~.

KEYWORDS: *ZnO nanorods, self-cleaning behaviour, static contact angle, roll-off angle, contact angle hysteresis.*

1. Introduction

A surface with a water contact angle greater than 150° and a roll-off angle less than 10° ~~are~~ **can be** considered to possess **an unique** ~~self-cleaning~~ superhydrophobic property. **Interestingly, this trait of superydrophoicity can be applied to self-cleaning process, which roots from the water repellent behaviour of naturally occurring lotus leaves** ~~This phenomenon of self-cleaning property is inspired from the naturally occurring water repellent behaviour of lotus leaves~~ [1-6]. Self-cleaning effect based on superhydrophobicity ~~is~~ **can be** defined as the **water droplet aided removal of dust particles** ~~removal of dust particles by the water droplet~~ at a small tilt angle ~~of the high water contact angle surfaces~~ [7-12]. ~~Self~~**Self-**cleaning surfaces are commercialized for **a number of** ~~various~~ applications**,** such as transparent and anti-reflective solar panel coatings [13, 14], self-cleaning windows [15-17], self-cleaning automobiles and coatings for architectures [16, 18, 19], solar absorber surfaces [20], electronic devices [21], anti-bio-fouling paints for boats ~~with drag reduction property~~[22] , snow and ice repellent coating for antennas and airplanes [23] and water/oil resistant protective coatings [24, 25, 26] **and so on**.

Several self-cleaning coatings based on ZnO have been developed in the past decades due to its unique optical and electrical properties. **At present,** ~~N~~**n**umerous synthesis methods and materials are available for the fabrication of ZnO based superhydrophobic self-cleaning coatings which include RF magnetron sputtering [27], electro-deposition approach [28], electrochemical processes [29], thermal evaporation [30, 31], thermal oxidation [32, 33], solution based approaches [34-38], MOCVD [39], nanocomposites [40, 41], lithography techniques [42] and ink-jet printing technique [43]. ~~It is clear that successful fabrication of several ZnO based self-cleaning surfaces have been made over the past decades, h~~**H**owever,

despite proactive efforts on fabrication, there ~~are still~~**exist number of** some unsolved challenges associated with these processes. ~~It~~ **These primarily** include**,**~~s~~ achieving large-scale, affordable, reproducible ZnO coatings for both conductive and non-conductive substrates for a wide range of applications.

For example, Badre et al. **[28]** deposited zinc oxide nanostructures on conductive F-doped SnO_2 coated glass using an electro - deposition technique for superhydrophobic self-cleaning applications ~~[28]~~. **Although promising,** ~~Though~~ the contact angle hysteresis of electrodeposited ZnO oxide is found to be 1°, this process is confined only to conductive surfaces. **Similary,** Xiong et al. **[39] efforts on** fabrica**tion of**~~ed~~ transparent zinc oxide based superhydrophobic coating for self-cleaning solar cells and displays using Metal Oxide Chemical Vapour Deposition (MOCVD) technique **appear** ~~This process is~~ constrained to **only** small size substrates; ~~hence, it may not be~~**a** cost **in**effective **technique** for **surfaces of** large ~~scale applications~~**dimensions**. **In response,** Myint et al. **[43]** produced ZnO nanorods with the combined use of ink jet printing and hydrothermal method for large area**s,** ~~applications~~ such as self-cleaning windows and sunroofs ~~[43]~~. This process of patterning has the drawback of **uncontrolled spread of ink which leads to** ~~spreading of ink to adjacent areas leading to~~ deterioration in the quality of patterned ~~growth of~~ nanorods**, making it a non-reproducible approach**~~; hence, it affects the reproducibility of coatings~~ [44].

Therefore, ~~T~~the present study focuses on developing a cost effective, low temperature synthesis **method for** ~~of~~ ZnO nanorods based self-cleaning coatings for glass substrates. **In the postulated technique,** ZnO nanorods based superhydrophobic surface ~~has~~ **have** been ~~developed~~ **produced over glass substrates** using **a** two-step solution based approach, namely SILAR (Successive Ionic Layer Adsorption and Reaction) and CBD (Chemical Bath Deposition)**, which is** followed by low surface energy modification. This two-step process is scalable to large area substrates **and** ~~. Moreover, it is~~ applicable to both conductive and non-

conductive substrates. Self-cleaning property of the superhydrophobic ZnO nanorods is assessed in terms of both high contact angle and low roll-off angle of water droplets. **Further the mechanism governing the low roll-off property of ZnO nanoroads coating, which is a key requirement for self-cleaning has been comprehensively explained using** ~~The mechanism associated with the easy roll-off of ZnO nanoroads coating is explained with the help of~~ an analytical model which **takes into account** ~~includes~~ both **surface chemistry and surface** structural features**.** ~~and surface chemical nature of the coatings.~~

2. Experimental Section

2.1. Synthesis of superhydrophobic ZnO coatings.

The glass slides (size: 75mm × 25mm; thickness: 1.3 mm) ~~are~~ **were** taken as a substrate**s, over which the** ~~for developing superhydrophobic~~ self-cleaning coatings **were developed.** Initially, the substrate is ultrasonically cleaned with acetone, ethanol, and double distilled (DD) water for 5 minutes to remove the organic contaminants from the substrate. **Briefly,** t~~T~~he superhydrophobic coatings based on ZnO nanorods ~~are~~ **were** prepared using the following three major steps: 1) Deposition of ZnO seed layer by Successive Ionic Layer Adsorption and Reaction (SILAR); 2) Growth of ZnO nanorods by Chemical Bath Deposition (CBD), and 3) Surface chemical modification through low surface energy silane solution.

Step-1: SILAR aided deposition of ZnO seed films. The seed layer deposition of ZnO thin films ~~is~~**was** prepared according to the procedure described elsewhere [45]. The SILAR deposition involves the four step process of successive reactions of cationic and anionic components at the ~~interface of the~~ substrate and ~~the~~ solution **interface**. Zinc sulphate heptahydrate (0.02 M, $ZnSO_4.7H_2O$, 99.5%, Merck) ~~is~~ **was** mixed with ammonium hydroxide solution (0.2M, NH_4OH, ~25%, Vetec) to obtain zinc ammonium complex ($[Zn(NH_3)_4]^{2+}$)**;** ~~solution~~, which then serves as cationic precursor. Double distilled (DD) water is heated close

to its boiling point ~~and it is~~was used as an anionic precursor. The four step process for the formation of ZnO seed layers are: (i) Immersion of cleaned substrates in zinc ammonia complex solution ($[Zn(NH_3)_4]^{2+}$) for 30-40 seconds to get adsorbed onto the glass substrate. (ii) ~~Immersion~~ Dispersion of ($[Zn(NH_3)_4]^{2+}$) adsorbed substrates into DD water for 20-30 seconds, where the adsorbed zinc ammonia complex ~~is~~ gets converted into zinc hydroxide ($Zn(OH)_2$). (iii) Ultrasonic agitation of $Zn(OH)_2$ coated substrates for around 60 seconds to remove the loosely bonded zinc hydroxide ($Zn(OH)_2$) molecules. (iv) Immersion of zinc hydroxide coated substrates into the water bath for 20-30 seconds, ~~which is~~ maintained at 80°C ~~for 20-30 seconds~~, where $Zn(OH)_2$ is converted into thin solid ZnO film. After completion of this cycle~~After completing a cycle of all the four processes~~, a drying period of 15-30 seconds ~~is~~ was maintained to enhance adhesion of successive layers of ZnO ~~seed layer~~ films. The whole deposition process ~~is~~ was repeated ~~up to~~for 20 cycles, in order to produce thick and adherent ZnO seed layers on the substrate. In order to eliminate left-over hydroxide phases, ~~T~~the substrate ~~is then~~was subsequently subjected to annealing process at 100°C for 60 minutes. ~~to achieve coatings without any hydroxide phases.~~ It must be underlined that the ~~The~~ SILAR deposited ZnO seed layers play an important role in offering nucleation sites for the growth of ZnO nanorods.

Step-2: CBD technique for the growth of ZnO nanorods. CBD technique is employed to grow ZnO nanorods on the seeded substrate [46]. Here, the seeded substrates were ~~is~~ immersed in an aqueous solution containing the equi-molar concentrations of zinc nitrate hexahydrate (0.1M, $Zn(NO_3)_2.6H_2O$, 96%, Merck) and hexamethylenetetramine (0.1M, $C_6H_{12}N_4$, 99%, Merck). The submerged substrates ~~immersed in the solution is~~were subjected to a temperature of 95°C, in hot air oven for nearly 3 hours. Finally, the substrates ~~are~~ were cleaned with DD water and acetone ~~for~~ several times to remove residual salts, and then dried at room temperature.

Step-3: Surface chemical modification of ZnO nanorods. The ZnO nanostructures thus grown ~~are~~ **were** chemically modified with 1H,1H,2H,2H perfluorooctyltriethoxysilane (PFOTES, CF_3 $(CF_2)_5$ $(CH_2)_2Si$ $(OCH_2CH_3)_3$, 97%, Alfa Aesar) using the dip coating method. The dipping and lifting speed of the substrate ~~is~~ **was** fixed at 50 mm/s. The contact time of substrate inside the solution ~~is~~ **was** maintained for 3 minutes**, which was later** ~~and then it is~~ annealed at 110°C for 30 minutes.

2.2. Characterization of ~~the~~ superhydrophobic ZnO nanorods.

The crystal structure, phase purity and growth direction of ZnO nanorods ~~are~~ **were** analysed using Grazing Incidence X-Ray Diffraction (GIXRD, Bruker D8 DISCOVER, Germany) and High Resolution Transmission Electron Microscope (HRTEM, JEOL JEM 2100). For HRTEM analysis, ZnO nanorods coating**s** **were**~~is~~ removed from its substrate by subjecting to ultrasonic treatment about 10 minutes ~~for dispersing it~~ in **an** ethanol medium. Finally, a few drops of that ethanol solution are dropped on the carbon coated copper grid for analysis. The surface morphology ~~is~~ **was** analysed using Field Emission Gun Scanning Electron Microscopy (FEGSEM, Carl Zeiss microscopy Ltd., UK & Sigma) and Atomic Force Microscopy (AFM, NTMDT, Russia).

The roughness features ~~are~~ **were** evaluated in a 10-µm square area of the AFM image using NOVA Image Analysis software (version: 1.0.26.1443). Sessile drop method and sessile drop needle-in method of contact angle measurement system (OCA15EC, Data Physics Instruments, Germany) ~~is~~ **were** used to determine the static and dynamic contact angles, respectively. For the contact angle measurements, the liquid used in the present study is double distilled water with constant volume of 10 µL. The contact angle measurements ~~are~~ **were** taken at minimum of five different places for each type of coatings. For dynamic contact angle (roll-off angle) measurements, the surface is placed at a particular angle and

then the droplet is placed over it. About 10 cycles of advancing and receding angle ~~are~~ **were** taken for analysis**,** and **the** ~~its~~ average value is considered as contact angle hysteresis.

Using the contact angle measurement system, the critical surface tension and relative polar-dispersive components of surface free energy ~~are~~ **were** evaluated using Zisman plot and Owens-Wendt-Rabel-Kaelble (OWRK's) method, respectively. For Zisman plot analysis, a set of liquids with wide range of surface tension such as water (γ_{LV}=72.75 mN/m), ethylene glycol (γ_{LV}=48 mN/m), benzene (γ_{LV}=28.65 mN/m) and toluene (γ_{LV}=28.40 mN/m) ~~are~~ **were** used. The liquids having diverse polar (γ_{LV}^{p}) and dispersive (γ_{LV}^{d}) surface energy components such as water (γ_{LV}=72.10 mN/m; γ_{LV}^{p}=52.20 mN/m; γ_{LV}^{d}=19.90 mN/m) and toluene (γ_{LV}=28.50 mN/m; γ_{LV}^{p}=1.32 mN/m; γ_{LV}^{d}=27.18 mN/m) ~~are~~ **were** used ~~for~~ **in the** Owens-Wendt-Ravel-Kaelble (OWRK's) approach.

3. Results and Discussion

3.1. Structural and morphological analysis

In order to examine the phase purity and growth direction of ZnO nanorods on glass substrates, the samples ~~are~~ **were** analysed using GIXRD**,** ~~and it is~~**as** shown in Fig. 1. The grown ZnO crystals are in hexagonal crystal structure [JCPDS # 36-1451] and ~~it~~ show~~s~~ sharp peak at 34.42°**,** which corresponds to (002) plane of hexagonal Wurtzite ZnO. All other reflections are perfectly matches with hexagonal ZnO structure**,** and no other impurity phases ~~are~~ **can be** identified ~~on the surface~~ [46, 47]. Low-magnification bright field TEM image ~~in~~ **(** Fig. 2a**)** depicts that the grown ZnO nanostructures have rod like structure and the Selected Area Electron Diffraction (SAED) in the inset in Fig. 2(a) **reflects the**~~shows that the~~ predominant direction of the growth of nanorods ~~is~~ **to be** [002]. Fig. 2(b) illustrate the HRTEM analysis of nanorods, which exhibit~~s~~ inter-planar spacing of 2.57 Å**;**~~,~~ closely ~~matches~~ **matching** with (002) plane of Wurtzite ZnO [JCPDS # 36-1451]. Elemental analysis of the corresponding ZnO nanorods is shown in Fig. 2(c). The spectra show the presence of

~~elements such as~~ Zn and O. The signature of Cu peak in the spectra is attributed to the use of copper grids for TEM analysis. **Therefore, to sum-up the**~~The~~ high intensity reflection of plane (002) from GIXRD and inter-planar spacing of 2.57 Å revealed from HRTEM analysis imply that the predominant growth of nanorods is towards [002] direction [46].

Figs. 3 and 4 show the morphology and distribution of the grown ZnO nanostructures**,** characterized using FESEM and AFM analysis, respectively. From the FESEM analysis in Fig. 3, it is identified that ZnO formed after CBD technique followed by silane coating have hexagonal prism like morphology with an average diameter of approximately 285 nm. **For comparison, the morphology of ZnO nanorods without silane coating was depiced in the Fig. S1 in supporting information.** Fig. 4 represents 3D AFM images of uncoated glass substrates (Fig. 4(a)), ZnO seeded substrates (Fig. 4(b)) and ZnO nanorods modified with silane (Fig. 4(c)).

Determination of statistical parameters plays an important role in the topographical characterization of a surface [48]. The statistical parameters for microscopic glass slides, ZnO seeded substrates and ZnO nanorods modified with silane are listed in Table 1. The statistical parameters, average roughness (S_a), RMS roughness (S_{rms}), peak to peak (maximum to minimum) height difference (S_y), ten point height difference (S_{10z}), Surface skewness (S_{sk}) and surface kurtosis (S_{ku}) are **all** incorporated in the analysis. The parameters, S_y and S_{10z} denote the extreme height differences of features of an image. The parameter S_y is more sensitive to noise than S_{10z}, since S_{10z} is the mean height difference between five local maxima and five local minima [48, 49]. For a reliable image, the S_{10z} value must be within 10-20% difference with S_y. From Table 1, it is evident that the difference in the values of S_y and S_{10z} lies within 20% for all the surfaces studied (glass substrates, ZnO seed layer and ZnO nanorods). It clearly demonstrates that the statistical parameters extracted from AFM images are free from noise and are reliable for analysis. S_a and S_{rms} are commonly used

roughness features for surface characterization. Table 1 show that there is an increasing trend in **the** values of average roughness (S_a) and RMS roughness (S_{rms}) from glass substrates through ZnO seed layers to ZnO nanorods coated with silane. This phenomenon is attributed to the formation of seed layers through SILAR process and the growth of nanorods through CBD technique [50-52]. Surface skewness, S_{sk} indicates the asymmetry in height distribution. The value of zero for S_{sk} indicates Gaussian-like surface distribution. Positive values of S_{sk} represent the domination of surface peaks over the pores. Consequently, the negative values indicate the domination of pores over the peaks. Positive value of S_{sk} for ZnO seed layer indicates that the surface is dominated by peaks, whereas ZnO nanorods grown by CBD technique followed by silane coating have negative values suggest that the surface is dominated by valleys (Table 1). The negative skewness parameter plays an important role in the wettability of surfaces.

Surface kurtosis, S_{ku} is an indicator of the peaks of the height distribution. The value of 3 for S_{ku} describes a Gaussian-like surface distribution. The distribution of surface with sharp peaks has the value greater than 3 and the one with a smoother top surface has the value less than 3. For ZnO seed layers, S_{ku} exceeds the value of 3 which indicates that the surface is largely covered with sharp peaks. On the other hand, ZnO nanorods coated with silane has S_{ku} value less than 3, suggests that the surface is covered with features with flat tops. ~~It~~ **This** is attributed to the hexagonal shaped top surface of grown ZnO nanorods. Thus, negative skewness value and the kurtosis value less than 3 for ZnO nanorods coated with silane (Table 1) support the FESEM results (Fig. 3) and it concludes that the surface is predominantly covered with valleys and the peaks have flat top surface.

3.2. Wettability studies

Fig. 5 shows the static and dynamic water contact angles measured on ZnO coated and uncoated substrates. The water droplet starts to spread quickly impact upon cleaned glass

substrates. Hence, the contact angle could not be measured precisely for those uncoated glass substrates ~~and~~**;** ~~it~~ **this** is evident in Fig. 5(a). After the seed layer deposition, the substrate shows hydrophobic behaviour with contact angle approaching 97° (Fig. 5(b)). The non-wettable behaviour is attributed to the increased roughness features (average roughness and RMS roughness)**,** when compared to uncoated glass substrate and ~~it~~ **this** is ~~evident~~ **apparent** from Table 1. Annealing of ZnO seeded substrate leads to the removal of impurity phase like Zn $(OH)_2$ and hence increase the contact angle to 105°**,** which is shown in Fig. 5(c). The annealing process burns off the -OH groups projecting from the surface. Thus, the decrease in polar groups of the surface increases the contact angle of water droplets on the surface [53].

The static contact angle of ZnO nanorods that are grown using CBD technique followed by silane surface modification has significantly increased to 155° and it is shown in Fig. 5(d). The synergy between **the** low surface energy of silane coatings and roughness features of ZnO nanorods are the reasons ~~to achieve~~**for** superhydrophobic property. **For comparison, glass substrate coated only with silane (absence of ZnO seed layer and ZnO nanorods) and glass substrate coated with ZnO nanorods over ZnO seed layer (absence of silane coating) were represented in the Fig. S2.** Another parameter which determines the wettability of solid surface is their surface free energy. There are many models to extract the surface free energy indirectly from the contact angle data [56-58]. In the present study, Zisman plot and Owens-Wendt-Rabel-Kaelble (OWRK'S) method ~~are~~ **were** adopted to calculate the critical surface tension and polar - dispersive components of total solid surface free energy, respectively. In Zisman method, the solid critical surface tension (γ_c) is calculated based on the experimental approach. **In accordence** to this approach, a series of probing liquids with successively decreasing surface tensions are used for the determination of static contact angles on the solid surface. When a liquid spreads on a surface with static contact angle of 0°, the surface tension of that liquid is equal to or less than the surface

energy of that solid surface. Zisman called this surface tension of liquid as the critical surface tension of that solid surface [59, 60]. In order to determine the critical surface tension of ZnO nanorods based superhydrophobic system, surface tension of several of probing liquids (with wide range of surface tension) and their cosine of the corresponding static contact angles are plotted as shown in Fig. 6. The solid line in the plot represents the best fit for the surface tensions of the liquid mediums used and the solid line is extrapolated upto contact angle of 0°, i.e., cos θ=1 [58, 59]. At the point of intersection (at cos θ=1), a perpendicular line is drawn to the X axis, it represents the critical surface tension of ZnO nanorods based superhydrophobic system and the value is calculated to be 12.44 mN/m. Thus, the liquids with surface tension less than or equal to 12.44 mN/m can completely wet the ZnO nanorods based superhydrophobic surface (i.e., at θ=0°). As the value of the critical surface tension decreases towards the left side of Zisman plot, the tendency of the water droplet to wet the solid surface decreases [58, 61], thereby it increases the contact angle value.

The OWRK's method is a geometric mean approach, which measures the polar and dispersive components of surface free energy of solid surface. This method is based on the molecular interactions between two substances at the contact interface [60]. According to this approach

$$\gamma_{LV}\cos\theta = 2\left[\gamma_{SV}^{d}\gamma_{LV}^{d} + \gamma_{SV}^{p}\gamma_{LV}^{p}\right] \quad (1)$$

$$\gamma_{SV} = \gamma_{SV}^{p} + \gamma_{SV}^{d} \quad (2)$$

where γ is the interfacial surface tension between two phases, S, L, V represents the solid, liquid, and vapour phase respectively, p and d represents relative polar and dispersive components of surface energy.

In order to calculate the surface free energy of solid surface based on OWRK's method, minimum of two liquids must be used. When substituting relative components of surface tension (γ_{LV}, γ_{LV}^{p}, γ_{LV}^{d}) of two liquids and their corresponding static contact angles (cos θ) on

the solid surface in the equation (1), the relative polar and dispersive components of surface free energy of that solid surface can be determined. Table 2 lists the polar, dispersive, total surface tensions of liquids used and the static contact angles of such liquids on ZnO nanorods based superhydrophobic surface. From the equation (1) and (2), the total surface free energy of the superhydrophobic ZnO nanorods is measured as 43.04 mN/m with dispersive components of 33.42 mN/m and polar components of 9.62 mN/m. The contact angle and surface energy of the solid substrate are inversely proportional to each other. As the surface polarity, i.e. the polar component of surface energy decreases, the affinity towards water decreases, thus leading to the increase in hydrophobicity [61]. For ZnO nanorods based superhydrophobic coating, the dispersive component of surface energy is higher when compared to polar component, indicating the poor pinning effect of water droplet to the superhydrophobic substrate [62, 63].

The roll-off angle (α) of glass substrate coated only with silane is to be measured as 55° which is shown in Fig. 7. Whereas the roll-off angle (α) and the contact angle hysteresis (Δθ) of silane coated ZnO nanorods grown glass substrate are measured to be as 1° and 2°, respectively. ~~It~~ **This** states that the roll-off angle of silane coated ZnO nanorods substrate is very low compared to silane coated glass substrate. The very low contact angle hysteresis of silane coated ZnO nanorod substrate is attributed to low pinning effect caused by the roughness features of nanorods [1]. Contact angle hysteresis represents the activation energy barrier offered by the substrate for the movement of water droplets. The long alkyl chain of silane groups freely rotates like a liquid layer on solid surfaces . The liquid like silane groups accompanied with roughness features causes free movement of **the** three phase contact line of contacting water droplets on such substrates, thus minimizing the activation barrier i.e. the corresponding contact angle hysteresis [64]. The smooth glass substrates coated with silane (absence of ZnO nanorods roughness features) may have low static contact angle and high

roll-off angle which is not sufficient to achieve superhydrophobic property. When smooth glass substrate is grown with ZnO nanorods and modified with silane groups, the static contact angle become high and the roll-off angle is reduced to minimum value, insisting the crucial role of roughness features for superhydrophobic property. Quere et al. **[65]** have proposed that in order to make the water droplet to roll on a surface, either the contact angle hysteresis must be minimized or static contact angle must be maximized ~~[65]~~. In the present study, both the conditions are satisfied by silane coated ZnO nanorods (contact angle of 155° and contact angle hysteresis of 2°) and this may be one of the reasons for its very low roll-off angle with water droplets.

3.3. Evaluation of self-cleaning effect

Substrates suitable for self-cleaning applications should have contact angle greater than 150° along with very low roll off angle (α) and contact angle hysteresis (Δθ) (both shoud be less than 5°) [15]. The ZnO nanorods based superhydrophobic surface prepared in this study satisfies aforementioned criteria**,** and hence its self-cleaning behaviour ~~is~~ **has been** investigated. For this, considerable amounts of saw dust are sprayed on the silane coated ZnO substrate and water droplet ~~is~~ **was** allowed to impact on the superhydrophobic surface. It is observed that water droplet removes off saw dust from such surface at a low roll-off angle of 1°. Fig. 8 show the adhesion of water droplet with saw dust particles on silane coated ZnO nanorods superhydrophobic substrate at horizontal position. The self-cleaning mechanism of ZnO superhydrophobic surface can be described as follows: When the size of dust particle is greater than the size of the surface features, the contact area between them is very small. **This would mean** ~~It shows~~ good adhesion between water droplets and saw dust, **i.e. individual surface energies to the substrate are high,** ~~in each case the individual surface energies to the substrate are relatively high~~, ~~as~~ **but** their combination reduces the global surface energy configuration. This explains the fact that why the dust particles adheres to the water droplet,

rolls off from the superhydrophobic surface at very low tilt angle**, thereby cleaning the surface**~~and makes the surface clean~~ [10].

3.4. Evaluation of roll-off angle on superhydrophobic surface

The low roll-off angle of water droplet is an important property to be achieved for superhydrophobicity based self-cleaning applications. In order to understand the mechanism behind low roll-off angle of various surfaces, several models have been proposed during the last five decades. In accordance with this, Frenkel [66] was the first to propose a relation among roll-off angle of a water droplet, droplet mass, surface tension and static contact angles and dynamic contact angle hysteresis of the droplet on a smooth surface. Furmidge [67] developed a common relation between the roll-off angle of the droplet and radius of the wetted area for smooth surface. Miwa et al. [68] extrapolated Furmidge equation for smooth surface to the rough surface by introducing the factor f, which is the fraction of solid surface in contact with droplet. Sakai et al. [69] developed a model to calculate the force which opposes the motion of droplets and compared the calculated values with the experimental results. Cunjing et al. [70] proposed an analytical model which relates the droplet parameters like surface tension, mass and volume, static contact angle with the roll-off angle. This model was utilized to explore the mechanism of roll-off of water droplets on pillar structured hydrophobic surfaces.

In the present study, to understand the effect of topological features and surface energy in determining roll-off angle, a simple model ~~is~~ **has been** developed based on force balance at the three phase contact line. In this model, ~~the~~ two surfaces are considered: 1) smooth surface ~~refers~~**referring** to the glass substrate coated only with silane having static contact angle of 105° and roll-off angle of 55°. 2) Rough surface ~~refers~~**referring** to silane coated ZnO nanorods glass substrate having static contact angle of 155° and roll-off angle of 1°. The former surface ~~shows~~ **exhibits** the effect of surface energy and the latter surface shows the

synergistic effect of morphological features as wells as surface energy in roll-off angle determination.

The following assumptions are made in the model:

1) Roll-off angle of smooth surface is less than or equal to 90°.
2) Experimental contact angle values are in time-invariant equilibrium.

At the onset of **water droplet** motion ~~of water droplet~~ on the tilted surface (Fig. 9), the force acting on the drop towards downward motion ($F_{gravity}$) i.e., gravitational force and the force opposing this motion ($F_{adhesion}$) i.e., adhesive forces are in equilibrium [71]. The gravitational force is given by

$$F_{gravity} = mg\sin\alpha \tag{3}$$

~~where~~ **Where,** α is the roll-off angle of water droplets on the solid surface, m is the mass of the water droplet and g is the acceleration due to gravity.

If the moment of rotation and frictional coefficient are ignored, adhesive force is given by

$$F_{Adhesion} = K\,2\pi r \tag{4}$$

$$r = R\sin\theta \tag{5}$$

~~w~~**W**here**,** r is the radius of the contact zone of water droplet on the surface, R is the radius of curvature of water droplet sitting on the solid surface and K is the interfacial energy with units of force/area (N/m). The interfacial energy is dependent on the chemical nature of the solid-vapour interface. Thus, irrespective of the physical status of the substrate used, the same interface energy is utilized for smooth and rough surfaces.

By assuming that the water droplet sits on the solid surface as a spherical cap of radius R (Fig. 10), the radius of curvature of droplet on the solid surface is calculated as a

function of mass (m) and density (ρ) of the liquid droplet used and the static contact angle (θ) of the droplet with the surface.

$$R=\left(\frac{3m}{\rho\pi\,(2-3\cos\theta+\cos^3\theta)}\right)^{\frac{1}{3}} \tag{6}$$

By incorporating experimentally observed static contact angle of smooth and rough solid surface, the corresponding radius of water droplet sitting on those surfaces can be obtained.

Combining equations (4), (5) and (6), the force of adhesion which opposes the movement of water droplet can be calculated from the radius of curvature of water droplet and its contact angle with solid substrate.

$$F_{Adhesion}=K\,2\pi\,R\sin\theta \tag{7}$$

Under equilibrium condition, the roll-off angle (α) for the smooth surface is calculated by equating the gravitational force (equation (3)) and the adhesion forces (equation (7)),

$$\sin\alpha=\left(\frac{K\,2\pi\,R\sin\theta}{mg}\right) \tag{8}$$

In the case of rough surfaces, the water droplet placed on the surface expected to sit only on the projected sites. Thus, the fraction of solid surface in contact with water droplet (f) must be included in the equation (8) for the calculation of roll-off angle of rough surface [65] and it is given by

$$\sin\alpha=\left(\frac{K\,2\pi\,f\,R\sin\theta}{mg}\right) \tag{9}$$

For nanorod surfaces, the factor, f, can be calculated using following expression from FESEM image in Fig.3 [69]:

$$f = \left(\frac{S_{head} \times \rho}{S_f} \right) \quad (10)$$

Where S_{head} is the top surface area of nanorods, ρ is the average number of nanorods per frame and S_f is the frame area in an image.

The variation in solid area fraction (f) (according to equation 10) with respect to average number of ZnO nanorods (ρ) and diameter of ZnO nanorods (d) is given in Fig. 11a and 11b, respectively. It is evident that the solid area fraction (f) increases linearly with average number of nanorods, whereas it exponentially increases with diameter of nanorods. The diameter of nanorods and average number of nanorods are inversely proportional to each other. Thus, in order to obtain low roll off angle, the diameter and average number of nanorods must be tuned in such a way that the obtained solid area fraction must be as small as possible. The theoretically calculated roll-off angle of water droplets on a superhydrophobic surface as a function of fraction of solid surface is given in Fig. 11c. From the Fig. 11c, it is observed that the slope of roll-off angle verses solid area fraction curve decreases with increase in static contact angle. If the density of the nanorods is too high or too low, the corresponding change in solid area fraction leads to a flat surface, which in turn reduces the contact angles and increases the roll-off angles. Hence a trade-off for solid area fraction should be realised for achieving high contact angle with low roll-off angle.

To assess the validity of the model, calculated roll-off angle values are compared with the experimental results reported in the literature [2, 69, 72, 73] and the result is depicted in the **Fig. S3, supporting information.** **Table S1 (in the supporting information)** lists the parameters obtained from the literature for calculating the roll-off angle. The plot between the calculated roll-off angle as a function of the solid area fraction of various superhydrophobic surfaces shows almost an expected and supporting trend, where roll-off angle decreases with

a decrease ~~in the~~ **with a decrease in the** solid area fraction. Moreover, the calculated results are closley matches with experimental results reported in the literature.

The model has been extended to predict the extremely low roll-off angle observed with ZnO superhydrophobic surface**, that has been** developed in the present study. For the calculation of roll-off angle of rough surface, the roll-off angle and static contact angle of smooth surface; and static contact angle of rough surface are obtained from the contact angle measurements. The fraction of solid surface in contact with water droplet for the rough surface is calculated from the FESEM image (frame size of 20μm×15μm) and it is found to be approximately around 9%. By substituting the contact angle values from Table 1 and the interfacial energy value (K), the roll-off is calculated to be around 3°, which is marginally higher than the experimental roll-off angle value of 1°. The deviation can be attributed to the over estimation of the area fraction of ZnO nanorods calculated based on FESEM analysis. When morphology of nanorod surface is analysed using FESEM, it may overlook the variation in the height of the ZnO nanorods and if water droplet sits only on the taller nanorods, it can roll-off very easily. In such condition, solid area fraction measured using FESEM analysis can mislead the analytical model and thus it may results in overestimation of roll-off angle. To overcome this problem, the fraction of taller nanorods to the total number of nanorods are calculated based on both the FESEM and AFM topographical images of ZnO nanorods and it is included in the calculation. In that case, the fraction of solid surface in contact with water droplet is around 5% and the corresponding theoretical roll-off angle is around 1°. Thus, by considering the topographical information from both FESEM and AFM analysis, the calculated roll-off angle value is in good agreement with experimental results.

4. Conclusion

A cost effective methodology for large scale production of ZnO nanorods based superhydrophobic surface has been developed on glass substrates. The synthesized surface have extremely low roll-off angle of around 1°. To understand the mechanism of roll-off angle, an analytical model have been developed, which predicts the roll-off angle of water droplets on nanorods by assuming the water droplet sits only on the taller nanorods. The diameter and density of the nanorods are varied in the model, which shows corresponding change in solid area fraction and the roll-off angles. If the density and diameter of nanorods are too low or high, it leads to a flat surface, which in turn reduces the contact angles and increases the roll-off angles. Hence, a trade-off for solid area fraction should be realised for achieving high contact angle with low roll-off angle. Validation of model has been done by comparison with reported literature and noted measurements.

Acknowledgements

The authors would like to thank Department of Science and Technology – Science and Engineering Research Board, Government of India under JC Bose National Fellowship (File. No. SR/S2/JCB-58/2011, 28.11.2011) for the financial support. The authors acknowledge Dr. S. Ilango and Dr. M. Kamruddin of Materials Science Group, Indira Gandhi Centre for Atomic Research, Kalpakkam for GIXRD characterization.

References

[1] R. Blossey, Self-cleaning surfaces- virtual realities, nature materials 2 (2003) 301-306.

[2] R. Furstner, W. Barthlott, C. Neinhuis, P. Walzel, Wetting and Self-Cleaning Properties of Artificial Superhydrophobic Surfaces, Langmuir 21 (2005) 956-961.

[3] Y. T. Cheng, D. E. Rodak, C. A. Wong, C. A. Hayden, Effects of micro- and nano-structures on the self-cleaning behaviour of lotus leaves, Nanotechnology 17 (2006) 1359-1362.

[4] N. Savage, Synthetic coatings: Super surfaces, 519 (2015) S7-S9.

[5] S. Yu, Z. Guo, W.Liu, Biomimetic transparent and superhydrophobic coatings: from nature and beyond nature, Chem. Commun., 51 (2015) :1775-1794.

[6] B. N. Sahoo, B. Kandasubramanian, Recent progress in fabrication and characterisation of hierarchical biomimetic superhydrophobic structures, RSC Adv.**, 4 (2014) 22053-22093.**

[7] V. A. Ganesh, H. K. Raut, A. S. Nair, A review on self-cleaning coatings, J. Mater. Chem. 21 (2011) 16304-16322.

[8] I. Sas, R. E. Gorga, J. A. Joines, K. A. Thoney, Literature Review on Superhydrophobic Self-Cleaning Surfaces Produced by Electrospinning, Journal of Polymer Science Part B: Polymer Physics 50 (2012) 824-845.

[9] J. Li, Z. Zhang, J. Xu, C. P. Wong, Self-cleaning Materials-Lotus effect surfaces, Kirk-Othmer Encyclopedia of Chemical Technology Wiley Blackwell: 11th volume, 2006.

[10] W. A. Daoud, Self-Cleaning Materials and Surfaces-A Nanotechnology Approach, 1st ed; John Wiley & Sons, Ltd., United Kingdom, 2013.

[11] N. M. Valipour, F. Ch. Birjandi, J. Sargolzaei, Super-non-wettable surfaces: A review, Colloids and Surfaces A: Physicochemical and Engineering Aspects 448 (2014) 93–106.

[12] Y.Y. Yan, N. Gao, W. Barthlott, Mimicking natural superhydrophobic surfaces and grasping the wetting process: A review on recent progress in preparing superhydrophobic surfaces, Advances in Colloid and Interface Science 169 (2011) 80–105.

[13] K. Askar, B. M. Phillips, Y. Fanga, B. Choia, N. Gozubenli, P. Jiang, Jiang, Self-assembled self-cleaning broadband anti-reflection coatings. Colloids and Surfaces A: Physico chem. Eng. Aspects 439 (2013) 84-100.

[14] L. Yao, J. He, Recent progress in antireflection and self-cleaning technology – From surface engineering to functional surfaces, Progress in Materials Science 61 (2014) 94–143.

[15] M. S. Jung, Natural and Biomimetic Artificial Surfaces for Superhydrophobicity, Self-Cleaning, Low Adhesion, and Drag Reduction. Ph.D. Thesis, The Ohio State University, Ohio, United States, 2009.

[16] X. Zhang, F. Shi, J. Niu, Y. Jiang, Z. Wang, Superhydrophobic surfaces: from structural control to functional application, J. Mater. Chem. 18 (2008), 621-633.

[17] X. Li, D. Reinhoudt, M. Crego-Calama, What do we need for a superhydrophobic surface? A review on the recent progress in the preparation of superhydrophobic surfaces, Chem. Soc. Rev., 36 (2007) 1350-1368.

[18] M. Zielecka, E. Bujnowska, Silicone-containing polymer matrices as protective coatings: Properties and applications, Progress in Organic Coatings 55 (2006) 160-167.

[19] P. Ragesh, V. A. Ganesh, S.V. Naira, A. S. Nair, A review on 'self-cleaning and multifunctional materials', J. Mater. Chem. A, 2 (2014) 14773-14797.

[20] H. C. Barshilia, , S. John, V. Mahajan, Nanometric multi-scale rough, transparent and anti-reflective ZnO superhydrophobic coatings on high

temperature solar absorber surfaces, Solar Energy Materials and Solar Cells, 107 (2012) 219–224.

[21] S. Lee, W. Kim, K. Yong, Overcoming The Water Vulnerability Of Electronic Devices: A Highly Water-Resistant ZnO Nanodevice With Multifunctionality, Adv. Mater., 23 (2011) 4398–4402.

[22] A. J. Scardino, H. Zhang, D. J. Cookson, R. N. Lamb, The role of nano-roughness in antifouling, Biofouling: The Journal of Bioadhesion and Biofilm Research 25 (2009) 757-767.

[23] T. Kako, A. Nakajima, H. Irie, Z. Kato, K. Uematsu, T. Watanabe, K. Hashimoto, Adhesion and sliding of wet snow on a super-hydrophobic surface with hydrophilic channels, Journal of Materials Science 39 (2003) 547-555.

[24] C. T. Hsieh, J. M. Chen, R. R. Kuo, T. S. Lin, C. F.Wu, Influence of surface roughness on water- and oil-repellent surfaces coated with nanoparticles, Applied Surface Science 240 (2005) 318-326.

[25] I. E. Palamà, S. D'Amone, V. Arcadio, D. Caschera, R. G. Toro, G. Gigli, B. Cortese, Underwater Wenzel and Cassie oleophobic behaviour, J. Mater. Chem. A, **3 (2015) 3854-3861.**

[26] C.Wang, F. Tzeng, H. Chen, C. Chang, Ultraviolet-Durable Superhydrophobic Zinc Oxide-Coated Mesh Films for Surface and Underwater–Oil Capture and Transportation, 28, Langmuir (2012) 10015–10019.

[27] Y. Liu, T. Tan, B. Wang, X. Song, E. Li, H. Wang, H. Yan, Superhydrophobic behavior on transparency and conductivity controllable ZnO/Zn films, Journal of Applied Physics 103 (2008) 056104-056106.

[28] C. Badre, T. Pauporte, M. Turmine, P. Dubot, D.Lincot, Water-repellent ZnO nanowires films obtained by octadecylsilane self-assembled monolayers, Physica E, 40 (2008) 2454-2456.

[29] T. Darmanin, E. T. Givenchy, S. Amigoni, F. Guittard, Superhydrophobic Surfaces by Electrochemical Processes, Advanced Materials 25 (2013) 1378–1394.

[30] U. P. Shaik, S. Kshirsagar, M. G. Krishna, S. P. Tewari, D. D. Purkayastha, V. Madhurima, Growth of superhydrophobic Zinc oxide nanowire thin films, Materials Letters 75 (2012) 51-53.

[31] U. P. Shaik, D. D. Purkayastha, M. G. Krishna, V. Madhurima, Nanostructured Zn and ZnO nanowire thin films for mechanical and self-cleaning applications, Applied Surface Science 330 (2015) 292–299.

[32] D. Sirbu, A. P. Rambu, G. I. Rusu, Microstructure, wettability and optical characteristics of ZnO/In2O3 thin films, Materials Science and Engineering B 176 (2011) 266-270.

[33] Z. Guo, X. Chen, J. Li, J. H. Liu, X. Huang, ZnO/CuO Hetero-Hierarchical Nanotrees Array: Hydrothermal Preparation and Self-Cleaning Properties, Langmuir 27 (2011) 6193–6200

[34] M. Afsal, L. J. Chen, Anomalous adhesive superhydrophobicity on aligned ZnO nanowire arrays grown on a lotus leaf, J. Mater. Chem. 21 (2011) 18061-18066.

[35] R. P. S. Chakradhar, V. D. Kumar, Water-repellent coatings prepared by modification of ZnO nanoparticles, Spectrochimica Acta Part A 94 (2012) 352-356.

[36] S. Sarkar, S. Patra, S. K. Bera, G. K. Paul, R. Ghosh, Water repellent ZnO nanowire arrays synthesized by simple solvothermal technique, Materials Letters 64 (2010) 460-462.

[37] C. L. Xu, L. Fang, F. Wu, Q. L. Huang, B. Yin, Wetting behavior of triethoxyoctylsilane modified ZnO nanowire films, Colloids and Surfaces A: Physicochemical and Engineering Aspects, 444, (2014) 48–53.

[38] J. Zhang, W. Huang, Y. Han, Wettability of Zinc Oxide Surfaces with Controllable Structures, 22 (2006) 2946–2950.

[39] J. Xiong, S. Das, B. Shin, J. P. Kar, J. H. Choi, J. M. Myoung, Biomimetic hierarchical ZnO structure with superhydrophobic and antireflective properties, Journal of Colloid and Interface Science 350 (2010) 344-347.

[40] R. P. S. Chakradhar, V. D. Kumar, J. L. Rao, B. J. Basu, Fabrication of superhydrophobic surfaces based on ZnO–PDMS nanocomposite coatings and study of its wetting behaviour, Applied Surface Science, 257 (2011) 8569–8575.

[41] Y. Liu, W. Chen, S. Wei, W. Gao, TiO_2/ZnO nanocomposite, ZnO/ZnO bi-level nanostructure and ZnO nanorod arrays: microstructure and time-affected wettability change in ambient conditions, RSC Adv., 4 (2014) 30658-30665.

[42] S. Dai, D. Zhang, Q. Shi, X. Han, S. Wang, Z. Du, Biomimetic fabrication and tunable wetting properties of three-dimensional hierarchical ZnO structures by combining soft lithography templated with lotus leaf and hydrothermal treatments, CrystEngComm., 15 (2013) 5417-5424.

[43] M. T. Z. Myint, R. Kitsomboonloha, S. Baruah, J. Dutta, Superhydrophobic surfaces using selected zinc oxide microrod growth on ink-jetted patterns, Journal of Colloid and Interface Science 354 (2011) 810-815.

[44] A. Dupuis, J. M. Yeomans, Modeling Droplets on Superhydrophobic Surfaces: Equilibrium States and Transitions, Langmuir 21 (2005) 2624-2629.

[45] P. Suresh Kumar, A. Dhayal Raj, D. Mangalaraj, D. Nataraj, N. Ponpandian, Lin Li, G. Chabrol, Growth of hierarchical based ZnO micro/nanostructured films and their tunable wettability behaviour, Applied Surface Science 257 (2011) 6678-6686.

[46] L. Vayssieres, K. Keis, S. E. Lindquist, A. Hagfeldt, Purpose-Built Anisotropic Metal Oxide Material: 3D Highly Oriented Microrod Array of ZnO. J. Phys. Chem. B 105 (2001) 3350-3352.

[47] S. Jung, E. Oh, K. Lee, W. Park, S. A. Jeong, Sonochemical Method for Fabricating Aligned ZnO Nanorods. Adv. Mater. 19 (2007) 749-753.

[48] J. Peltonen, M. Jarn, S. Areva, M. Linden, J. B. Rosenholm, Topographical Parameters for Specifying a Three-Dimensional Surface, Langmuir 20 (2004) 9428-9431.

[49] K. J. Stout, P.J. Sullivan, W. P. Dong, E. Mainsah, N. Luo, T. Mathia, H. Zahouani, The development of methods for the characterisation of roughness in three Dimensions, Commission of the European Communities: Luzemburg, 1993.

[50] L. B. Boinovich, A. M. Emelyanenko, A. S. Pashinin, C. H. Lee, J. Drelich, Y.K. Yap, Origins of Thermodynamically Stable Superhydrophobicity of Boron Nitride Nanotubes Coatings, Langmuir 28 (2012) 1206-1216.

[51] K. L. Cho, I. I. Liaw, A. H. F. Wu, R. N. Lamb, Influence of Roughness on a Transparent Superhydrophobic Coating, J. Phys. Chem.C 114 (2010) 11228-11233.

[52] A. Sugunan, H. C. Warad, M. Boman, J. Dutta, Zinc oxide nanowires in chemical bath on seeded substrates: Role of hexamine, J Sol-Gel SciTechn 39 (2006) 49-56.

[53] J. Bico, U. Thiele, D. Quere, Wetting of textured surfaces, Colloids and Surfaces A: Physicochemical and Engineering Aspects 206 (2002) 41-46.

[54] Z. Guo, W. Liu, Sticky superhydrophobic surface, Appl. Phys. Lett. 90 (2007) 223111-223113.

[55] D. Quere, A. Lafuma, J. Bico, Slippy and sticky microtextured solids, Nanotechnology. 14 (2003) 1109-1112.

[56] F. Hejda, P. Solar, J. Kousal, Surface Free Energy Determination by Contact Angle Measurements – A Comparison of Various Approaches, WDS'10 Proceedings of Contributed Papers 2010, pp 25-30.

[57] M. Zenkiewicz, New method of analysis of the surface free energy of polymeric materials calculated with Owens-Wendt and Neumann methods, Polimery 51 (2006) 584-587.

[58] M. Levine, G. Ilkka, P. Weiss, Relation of the critical surface tension of polymers to adhesion, Polymer letters 2 (1964) 913-919.

[59] H. W. Fox, W. A. Zisman, The spreading of liquids on low energy surfaces. I. Polytetrafluoroethylene. Journal of Colloid Science 5 (1950) 514-531.

[60] Owens, D. K. Estimation of the Surface Free Energy of Polymers. Journal of Applied Polymer Science 13 (1969) 1741-1747.

[61] G. Azimi, R. Dhiman, H. Kwon, A. T. Paxson, K. K. Varanasi, Hydrophobicity of rare-earth oxide ceramics. Nature Materials 12 (2013) 314-320.

[62] B. Janczuk, E. Chibowski, M. Hajnos, T. Biaeopiotrowicz, J. Stawinski, Influence of exchangeable cations on the surface free energy of Kaolinite as determined from contact angles, Clays and Clay Minerals 37 (1989) 269-272.

[63] A. M. Munshi, V. N. Singh, M. Kumar, J. P. Singh, Effect of nanoparticle size on sessile droplet contact angle, Journal of Applied Physics 103 (2008) 084315-084319.

[64] L. Gao, T. J. McCarthy, Contact Angle Hysteresis Explained, Langmuir 22 (2006) 6234-6237.

[65] D. Quere, fakir droplets, nature materials 1 (2002) 14-15.

[66] Y. I. Frenkel, On the behavior of liquid drops on a solid surface The sliding of drops on an inclined surface, J. Exptl. Theoret. Phys. (USSR) 18 (1948) 659-668.

[67] C. G. L. Furmidge, Studies at phase interfaces I. The sliding of liquid drops on solid surfaces and a theory for spray retention, Journal of Colloid Science 17 (1962) 309-324.

[68] M. Miwa, A. Nakajima, A. Fujishima, K. Hashimoto, T. Watanabe, Effects of the Surface Roughness on Sliding Angles of Water Droplets on Superhydrophobic Surfaces Langmuir 16 (2000) 5754-5760.

[69] M. Sakai, K. Kono, A. Nakajima, X. Zhang, H. Sakai, M. Abe, A. Fujishima, Sliding of Water Droplets on the Superhydrophobic Surface with ZnO Nanorods Langmuir 25 (2009) 14182-14186.

[70] C. Lv, C. Yang, P. Hao, F. He, Q. Zheng, Sliding of Water Droplets on Microstructured Hydrophobic Surfaces Langmuir 26 (2010) 8704-8708.

[71] H. Murase, T. Fujibayashi, Characterization of molecular interfaces in hydrophobic systems Progress in Organic Coatings 3(1) (1997) 97-107.

[72] P. F. Rios, H. Dodiuk, S. Kenig, S. Mccarthy, A. J. Dotan, The effects of nanostructure and composition on the hydrophobic properties of solid surfaces, Adhesion Sci. Technol. 20 (2006) 563-587.

[73] Y. Kwon, N. Patankar, J. Choi, J. Lee, Design of Surface Hierarchy for Extreme Hydrophobicity, Langmuir 25 (2009) 6129-6136.

Figure captions

Fig. 1. GIXRD analysis of ZnO nanorods.

Fig. 2. a) TEM bright field image (Inset: SAED pattern). b) HRTEM analysis (Inset: FFT image). c) Elemental analysis of ZnO nanorods.

Fig. 3. FESEM image of CBD grown ZnO nanorods coated with silane

Fig. 4. 3D AFM images of a) cleaned glass substrates, b) ZnO seeded substrates and c) ZnO nanorods modified with silane coating.

Fig.5. Static water contact angle measurements of a) cleaned glass substrate. b) un-annealed ZnO seed layer. c) annealed ZnO seed layer . d) ZnO nanorods with silane coatings.

Fig. 6. Zisman plot for superhydrophobic ZnO nanorods.

Fig. 7. Dynamic contact angle (Roll-off angle, α) of bare glass substrate coated with silane.

Fig. 8. Self-cleaning effect on ZnO nanorods modified with silane coatings

Fig. 9. Roll-off motion of water droplet in tilted substrate

Fig.10. Liquid droplet on a solid substrate as a spherical cap with radius of curvature R, makes an angle θ with the substrate. The radius of the contact area of solid –liquid interface is r.

Fig. 11. Variation of solid area fraction with respect to (a) Average diameter of nanorods (d) and (b) Average number of nanorods (ρ) ; (c) Variation of roll-off angle of water droplet with respect to the solid area fraction.

Table captions

1. Comparison of statistical parameters and contact angle values of substrates

2. OWRK's method data: Surface tension components of liquids and their corresponding static contact angles on ZnO nanorods based superhydrophobic surface.

Fig. 1

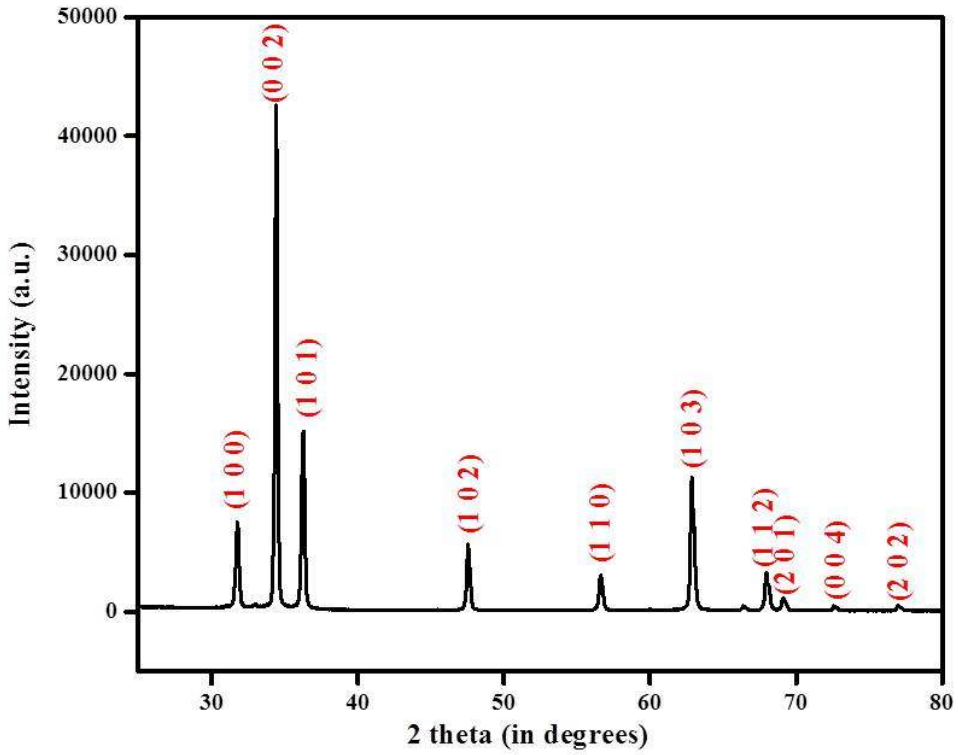
Intensity (a.u.)
2 theta (in degrees)
(1 0 0)
(0 0 2)
(1 0 1)
(1 0 2)
(1 1 0)
(1 0 3)
(1 1 2)
(2 0 1)
(0 0 4)
(2 0 2)

Fig. 2

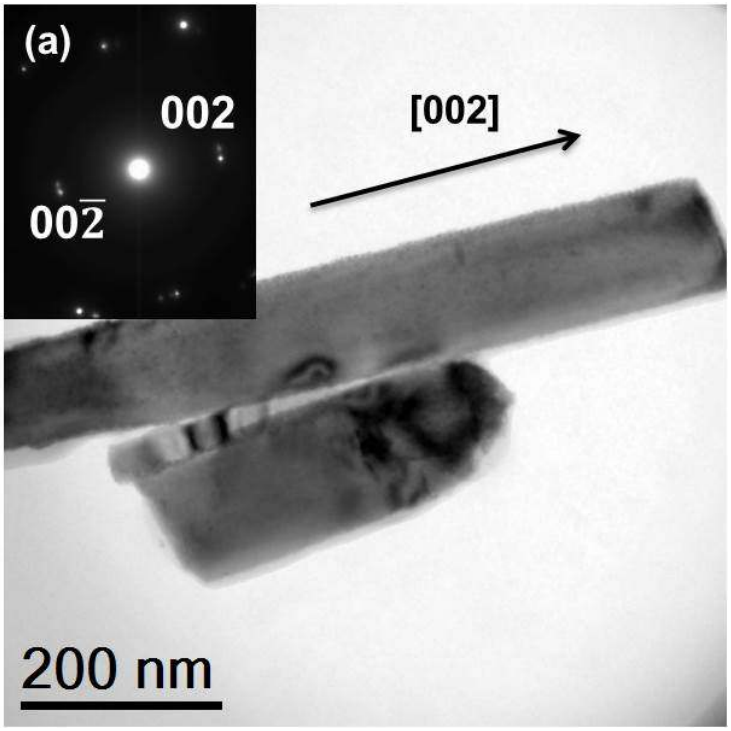
(a)
002
00$\bar{2}$
[002]
200 nm

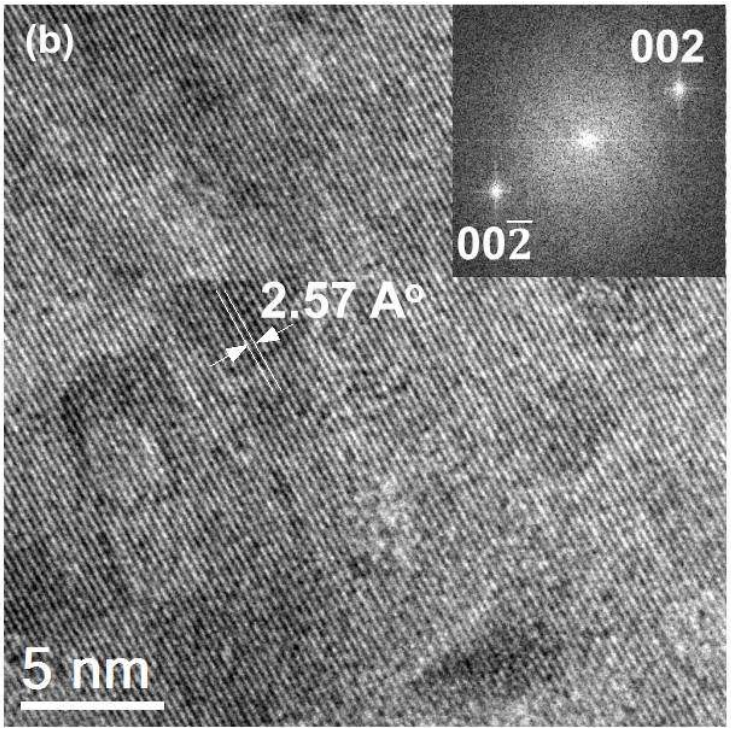
(b)
002
00$\bar{2}$
2.57 A°
5 nm

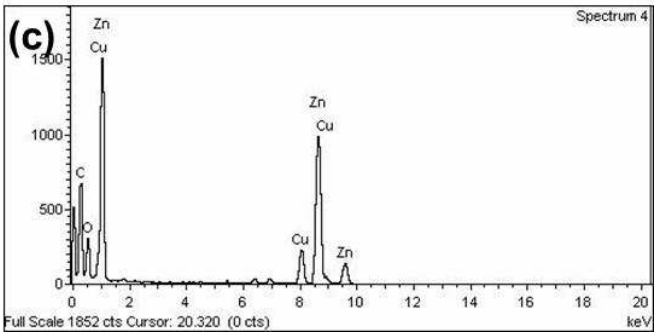
(c)
Spectrum 4
Zn
Cu
Zn
Cu
C
O
Cu
Zn
1500
1000
500
0
0
2
4
6
8
10
12
14
16
18
20
Full Scale 1852 cts Cursor: 20.320 (0 cts)
keV

Fig. 3

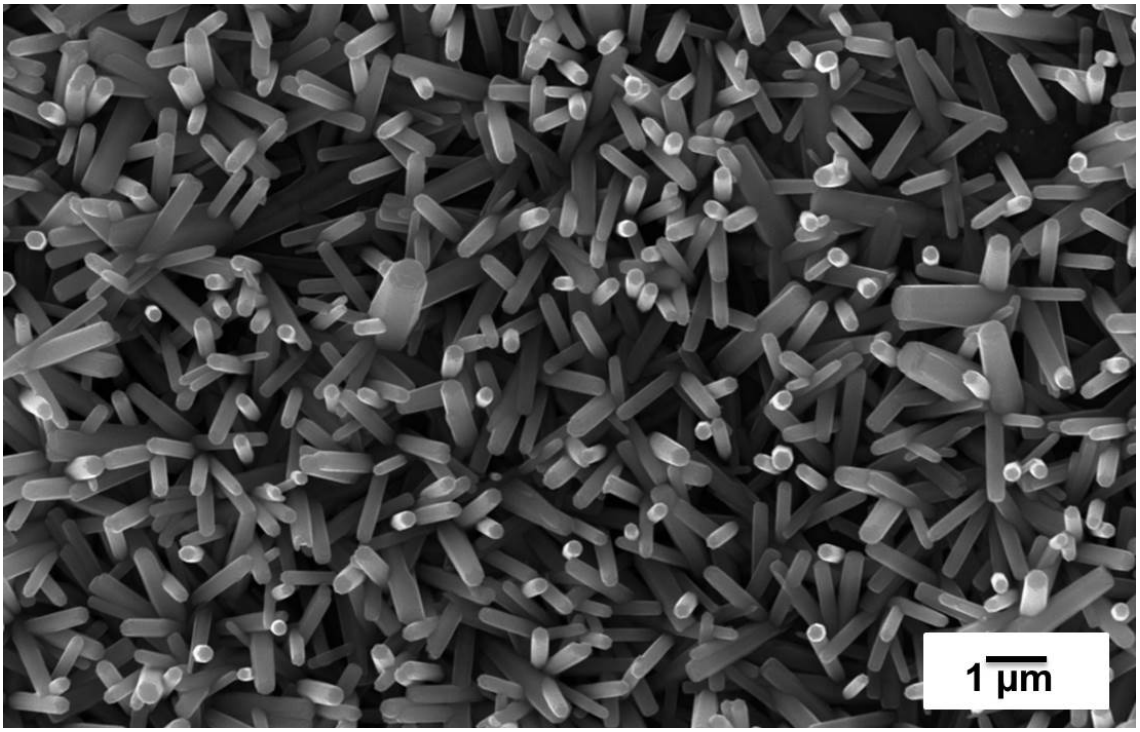

Fig. 4

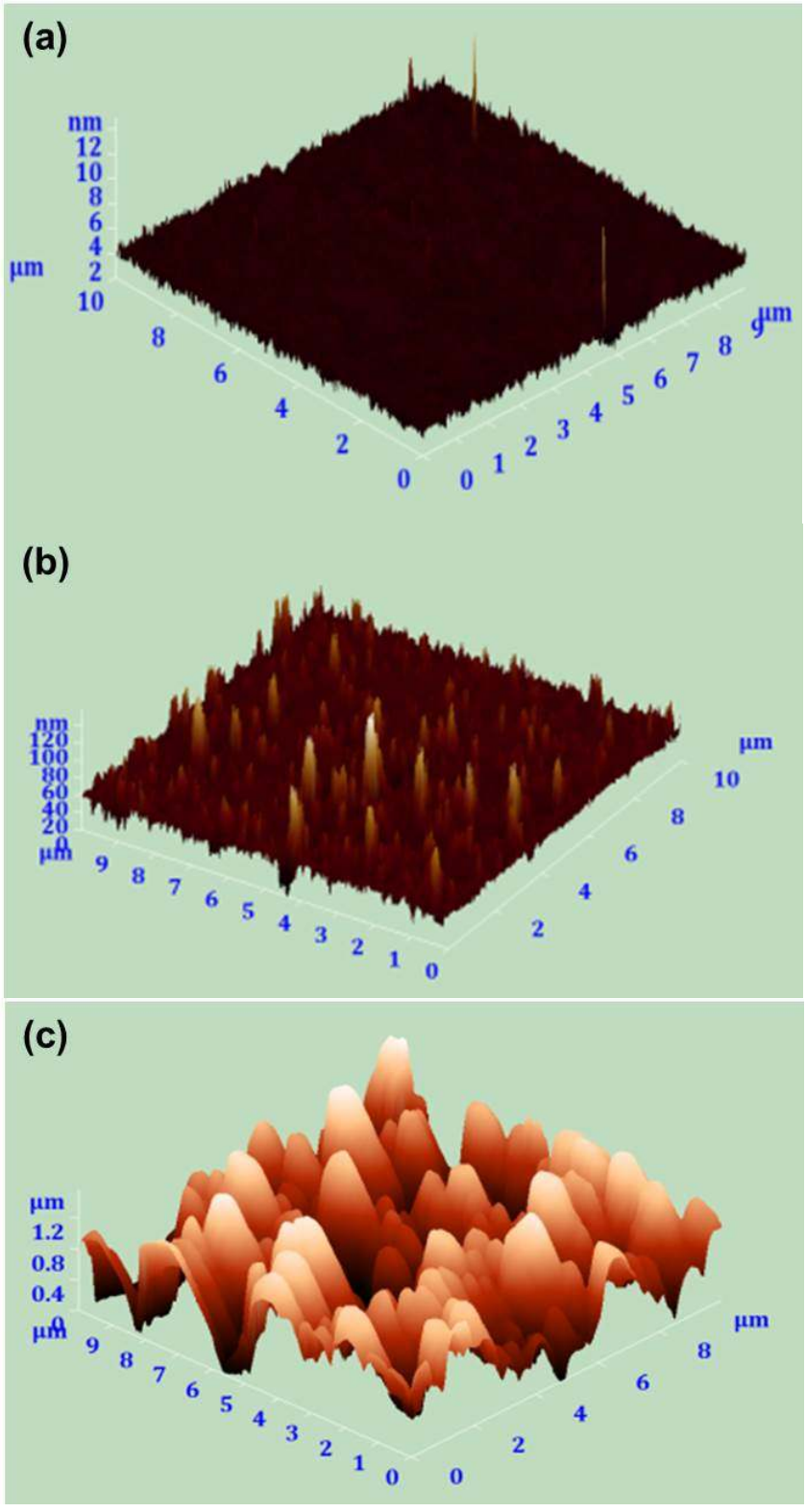
(a)
nm
12
10
8
6
4
2
0
µm
10
8
6
4
2
0
0
1
2
3
4
5
6
7
8
9
µm
(b)
nm
120
100
80
60
40
20
0
µm
9
8
7
6
5
4
3
2
1
0
2
4
6
8
10
µm
(c)
µm
1.2
0.8
0.4
0
µm
9
8
7
6
5
4
3
2
1
0
0
2
4
6
8
µm

Fig. 5

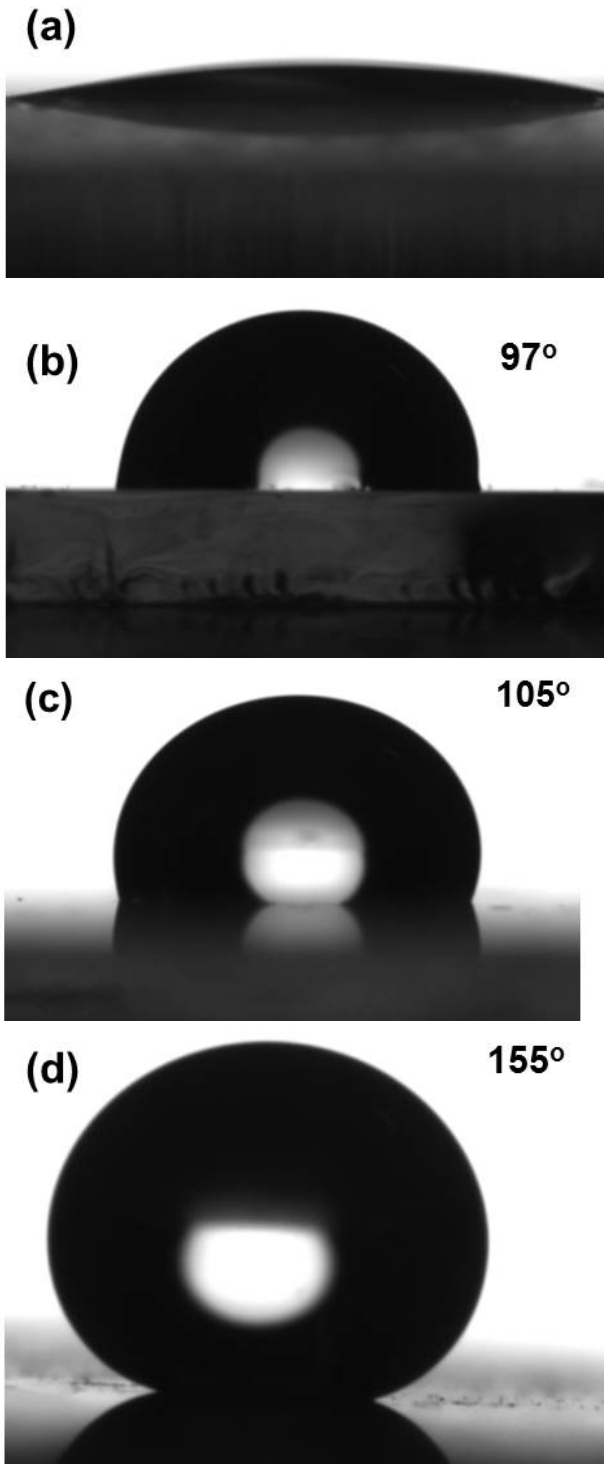

Fig. 6

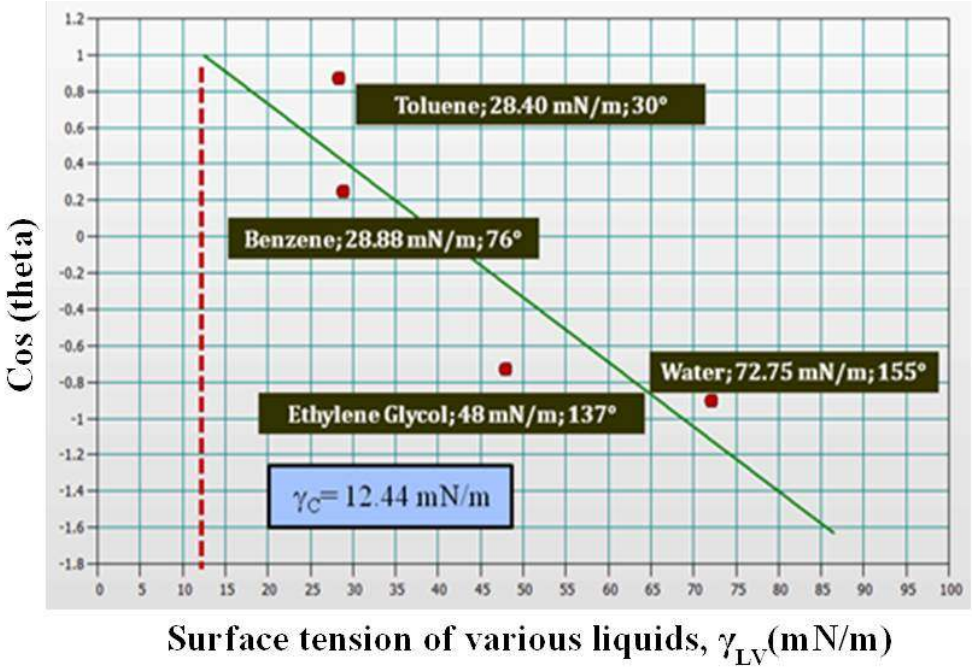
Toluene; 28.40 mN/m; 30°
Benzene; 28.88 mN/m; 76°
Water; 72.75 mN/m; 155°
Ethylene Glycol; 48 mN/m; 137°
γ_C= 12.44 mN/m
Cos (theta)
Surface tension of various liquids, γ_{LV}(mN/m)

Fig. 7

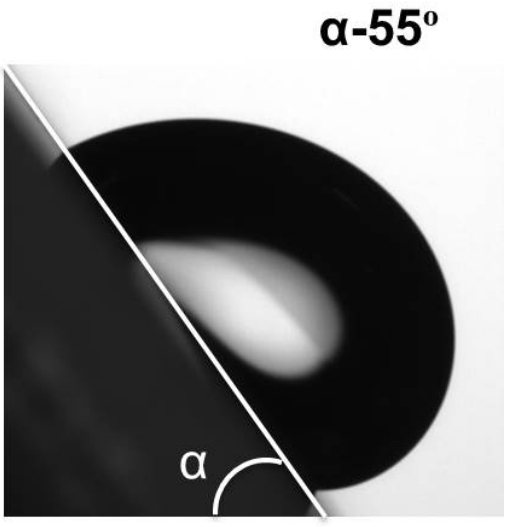
α-55°
α

Fig. 8

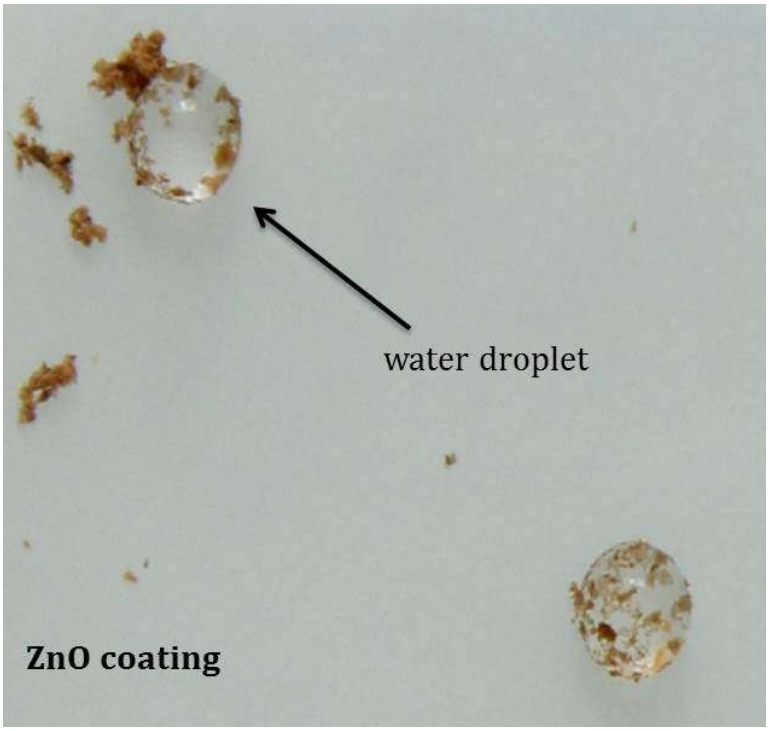

Fig. 9

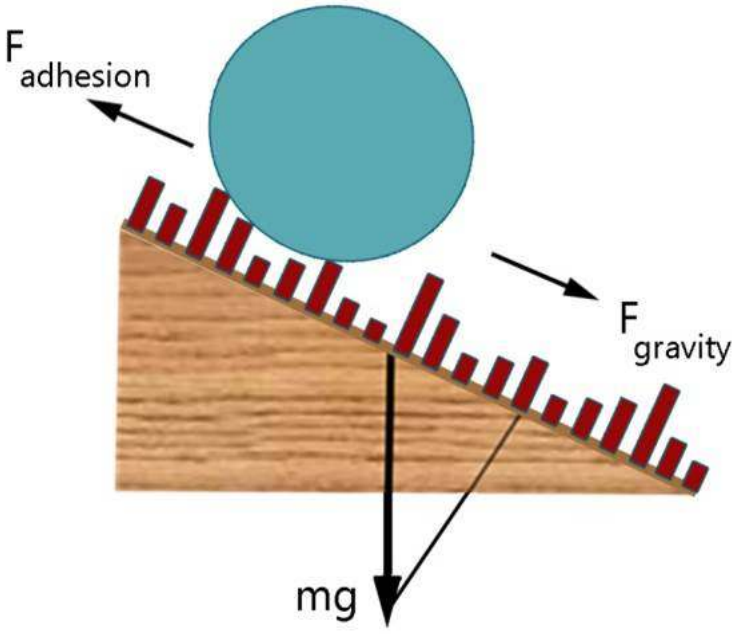

Fig. 10

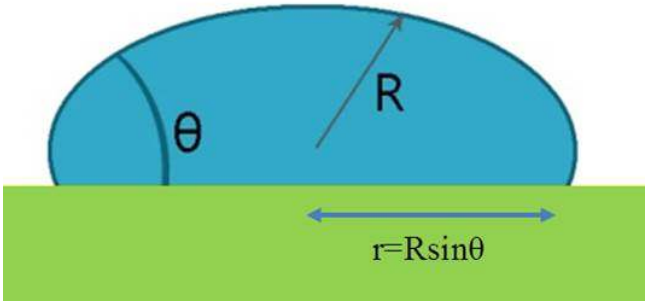

Fig. 11

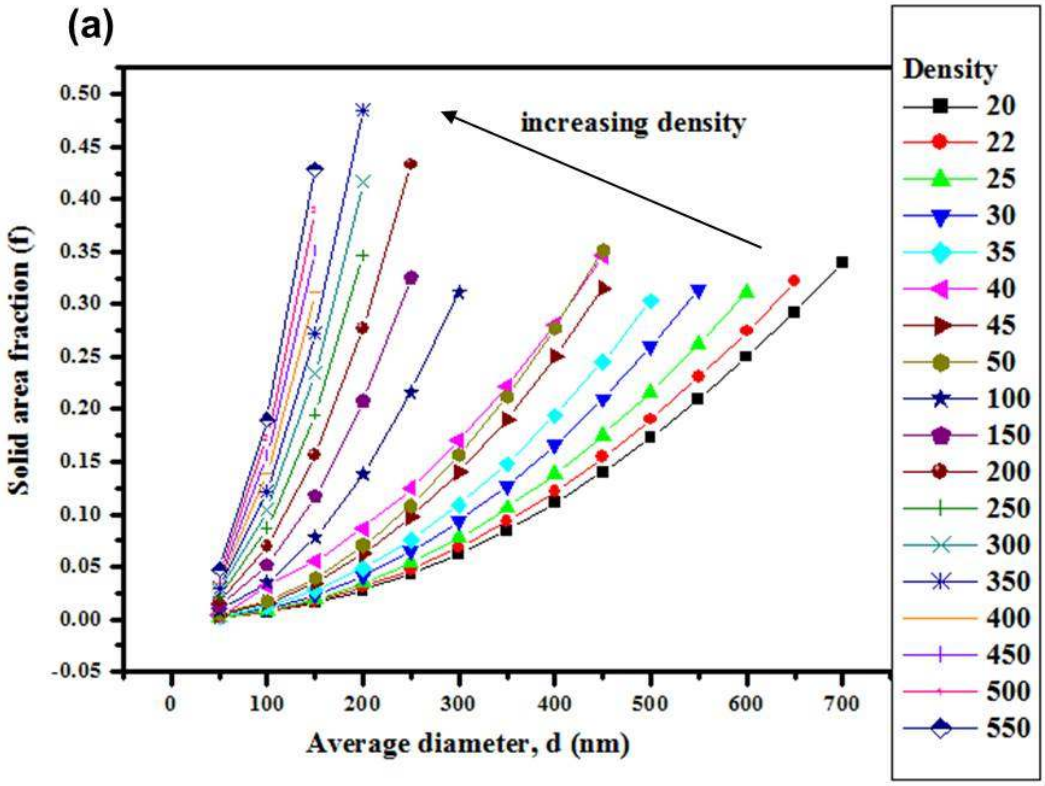
(a)
Solid area fraction (f)
Average diameter, d (nm)
increasing density
Density
20
22
25
30
35
40
45
50
100
150
200
250
300
350
400
450
500
550

(b)

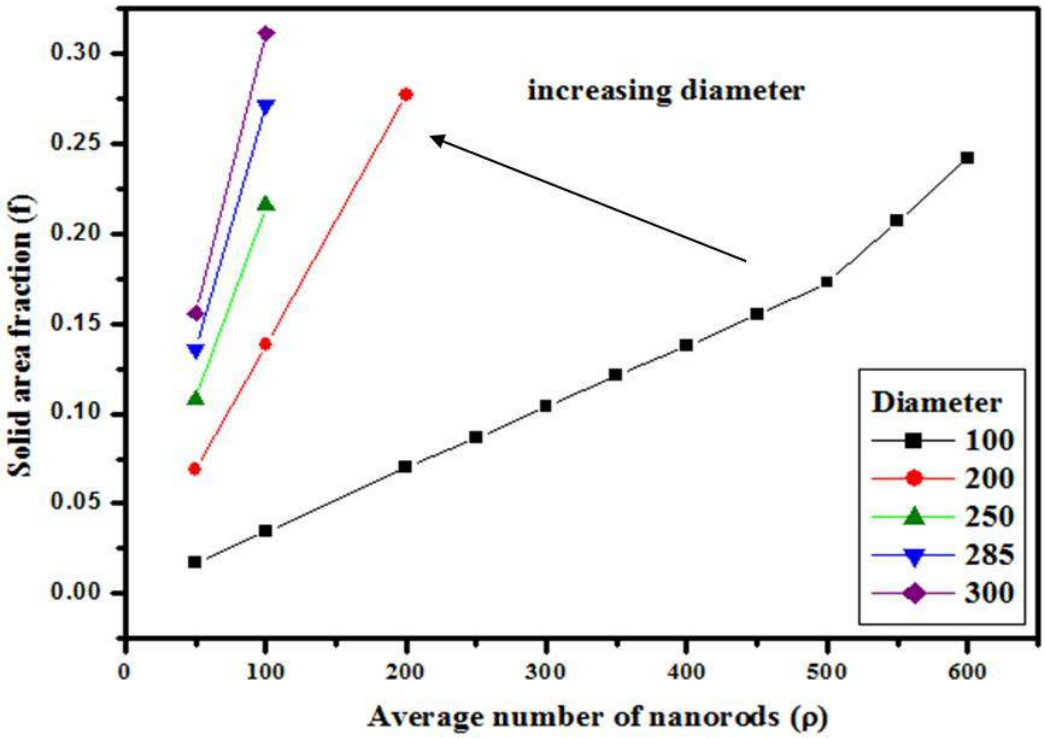
increasing diameter
Solid area fraction (f)
Average number of nanorods (ρ)
Diameter
100
200
250
285
300
0.00
0.05
0.10
0.15
0.20
0.25
0.30
0
100
200
300
400
500
600

(c)

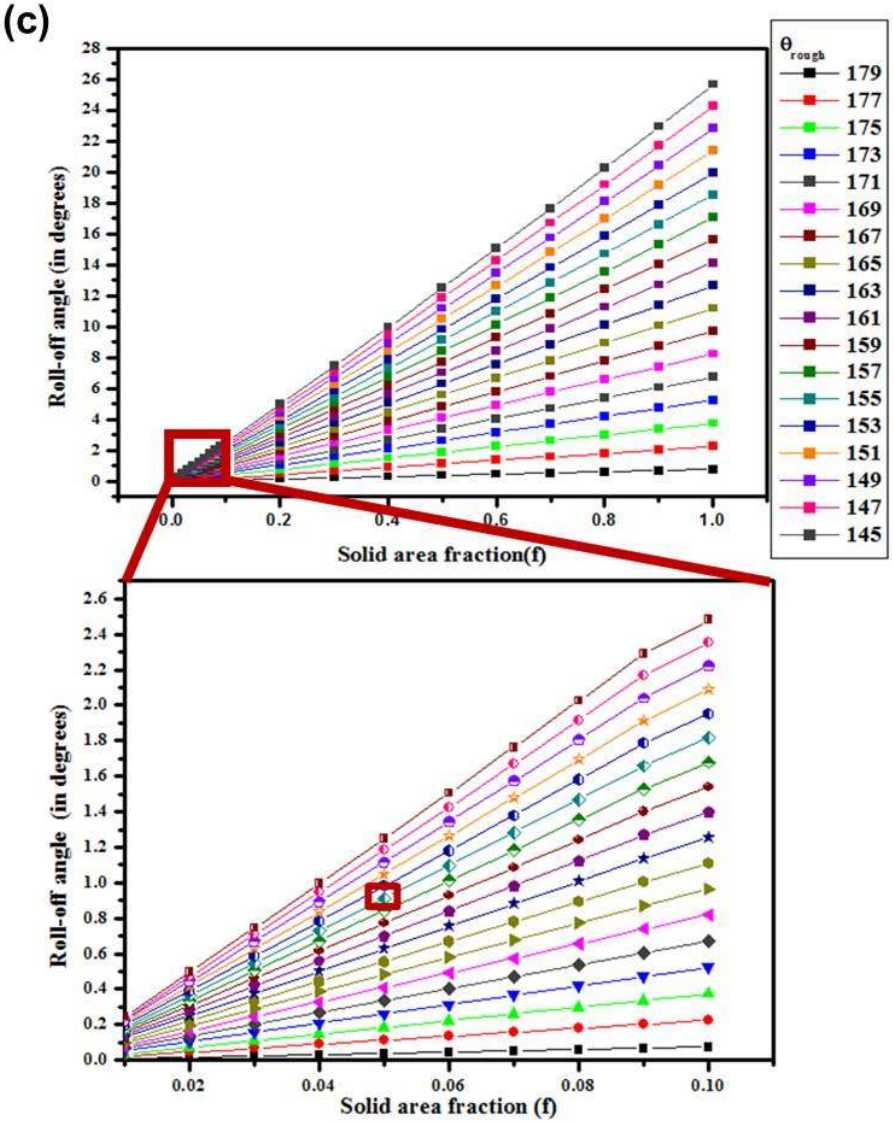
θ rough
179
177
175
173
171
169
167
165
163
161
159
157
155
153
151
149
147
145
Roll-off angle (in degrees)
Solid area fraction(f)
Roll-off angle (in degrees)
Solid area fraction (f)

Table 1

Substrates	Micro-scopic glass	ZnO seed layer	ZnO nanorods coated with silane
S_a, Average roughness (nm)	1.5558	5.2458	333.59
S_{rms}, RMS roughness (nm)	1.8467	8.7379	396.37
S_y, Peak to peak height (nm)	17.052	133.63	1797.4
S_{10Z}, Ten point height (nm)	12.627	119.04	1615.7
S_{sk}, Surface skewness	0.0307	3.6607	-0.079
S_{ku}, Surface kurtosis	2.2403	28.99	2.422
Static contact angle (°)	-	105	155
Roll off angle (°)	-	55	1
Contact angle hysteresis (°)	-	-	2

Table2

Liquids used	Total surface tension, γ_{LV}(mN/m)	Polar component of Surface tension, γ_{LV}^{P} (mN/m)	Dispersive component of surface tension, γ_{LV}^{d} (mN/m)	Static contact angle (°)
Water	72.10	52.20	19.90	155
Toluene	28.50	1.32	27.18	30